

SEISMIC REEVALUATION OF A FUEL STORAGE RACK CONSIDERING FSI AND FRICTION EFFECTS

Stefan Riedelmeier¹, Holger Senechal²

¹ Simulation Engineer, KAE GmbH, Hausen, Germany
(riedelmeier@kae-gmbh.de)

² Structural Engineer, KAE GmbH, Hausen, Germany

ABSTRACT

The subject of the paper is the seismic reevaluation of a fuel storage rack considering FSI (Fluid-Structure Interaction) and friction effects. Due to new earthquake hazard, new acceleration-time-histories for the fuel pool were determined. A non-linear transient Finite Element Analysis is performed, at which various accelerations-time-histories are considered. Although, the new maximum accelerations are nearly 3 times higher than for the design of the fuel storage rack, for each acceleration-time-history, no collisions with the pool wall or other racks occur. The maximum relative displacements are even smaller than for the design calculation. Additionally, no severe tilting is observed and the maximum stresses are below the allowable stresses.

MOTIVATION

As a consequence of the Fukushima accident in 2011 (IAEA (2015)), new acceleration time histories and floor response spectra for a lot of nuclear power plants were determined. Generally, this results in higher accelerations. Hence, a seismic reevaluation of components is necessary. In order to obtain a positive proof conservatism has to be reduced and effects such as FSI have to be considered.

DYNAMIC PRESSURES IN POOLS DURING EARTHQUAKE

Generally, the dynamic pressures in pools during earthquake are divided into an impulsive and a convective part (DIN EN 1998-4 (2007)). The dynamic pressures are caused by the pool motion, which of course is a result of the building motion.

The convective part represents the sloshing of the free surface of the fluid. Considering fuel pools, which are relatively deep, the sloshing is generally localized in the very top region of the pool. The first sloshing frequency f_1 is calculated using Equation (1) (DIN EN 1998-4 (2007)).

$$f_1 = \left\{ 2\pi \left[\frac{L/g}{0.5\pi \tanh\left(0.5\pi \frac{H}{L}\right)} \right]^{0.5} \right\}^{-1} \quad (1)$$

The parameter L is the half of the width of the pool in direction of excitation, g is the gravitational acceleration and H is the height of the fuel pool in relation to the fluid surface. Consequently, sloshing frequencies are a type of natural frequencies. In order to quantify the convective pressure, you need amongst others the excitation acceleration at the sloshing frequency.

The impulsive part represents pressure waves caused by the change in velocity of the pool wall during earthquake. When a pool is accelerated in horizontal direction with acceleration a , impulsive

pressures are generated at the pool wall (see Figure 1). The positive change in pressure is indicated with $+\Delta p$ and the negative change in pressure is indicated with $-\Delta p$. In the pool center the change in pressure is zero due to the superposition of high and low pressure waves. The impulsive pressures travel at the speed of sound of the fluid. The theoretical upper limit of the impulsive pressure is given by the Joukowsky Equation (Equation (2), Joukowsky (1898)), where ρ is the fluid density, c is the speed of sound and Δv is the change in velocity. But it has to be mentioned, that generally the impulsive pressures are much smaller than the full Joukowsky pressure amplitude.

$$\Delta p = \rho c \Delta v \quad (2)$$

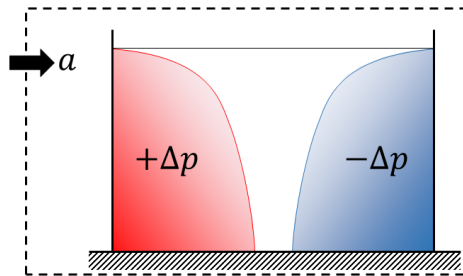


Figure 1: Schematic distribution of the impulsive pressure in case of acceleration of the pool

FSI

The dynamic pressures, caused by pool motion (also FSI effect), excite fuel storage racks standing on the pool ground (mainly the impulsive part). The bigger the dimension of the rack in the direction of excitation and the bigger the effective pressure area, the bigger is this effect. On the other, the racks are also excited directly via the motion of the pool ground (friction between rack and ground). When the fuel storage rack moves in relation to the pool ground – either by slipping or by natural oscillations – the relative motions cause pressure waves in the fluid, which vice versa have an impact on the motion of the structure. The effect of the fluid on the structure can be described using added mass, damping and stiffness (i.e. A. S. Dehkharghani et al. (2018)), where the added stiffness in case of fuel storage racks can be neglected. Hence, the main effects for the structure are added mass and damping, which means basically that the natural frequencies of the fuel storage racks are reduced.

FUEL STORAGE RACK

The basic setup of the fuel storage rack is shown in Figure 2. The main components are the insert frames, the fuel element channels, the base plate including the substructure and the pedestals. The racks stand on the pool ground without mounting. Each rack has 10x8 channels. The fuel element channels are only mounted on the base plate of the rack – there is no other coupling between the channels. The fuel elements are fixed with pins to the bottom part of the fuel element channels. The main dimensions of the fuel storage rack are length x width x height = 2420 mm x 1930 mm x 3990 mm. In total there are 4 racks on the ground of the pool. The distance between the racks is 200 mm and the minimum distance between a rack and the pool wall is 500 mm.

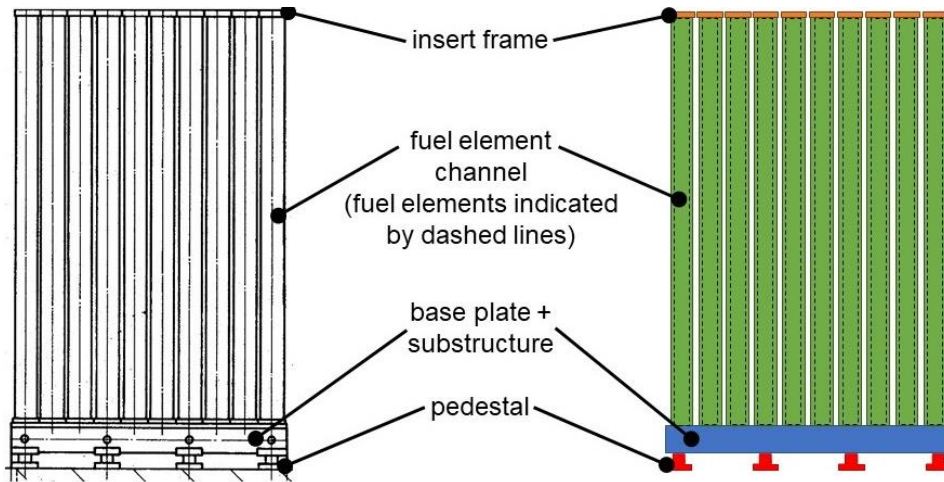


Figure 2: Basic setup of the fuel storage racks

FUEL POOL

The pool is quad-shaped and has the main dimensions length x width x height = 7870 mm x 6540 mm x 9870 mm. The height is related to the free surface of the fluid.

EARTHQUAKE EXCITATION

The excitation represents floor response spectra for the fuel pool ground (Figure 3). The peak accelerations have values of $2.6g$ (4.4 Hz) in x -direction, $2.1g$ (4.2 Hz) in y -direction and $2.0g$ (6.5 Hz) in z -direction. Based on the floor response spectra spectra-compatible acceleration-time-histories for the pool are generated. According to KTA 2201.1 (2011) for nonlinear problems a set of 7 acceleration-time-histories (x, y, z) has to be considered. The rigid body acceleration in the horizontal direction is ca. $0.6g$, which is nearly 3 times higher compared to the design calculation.

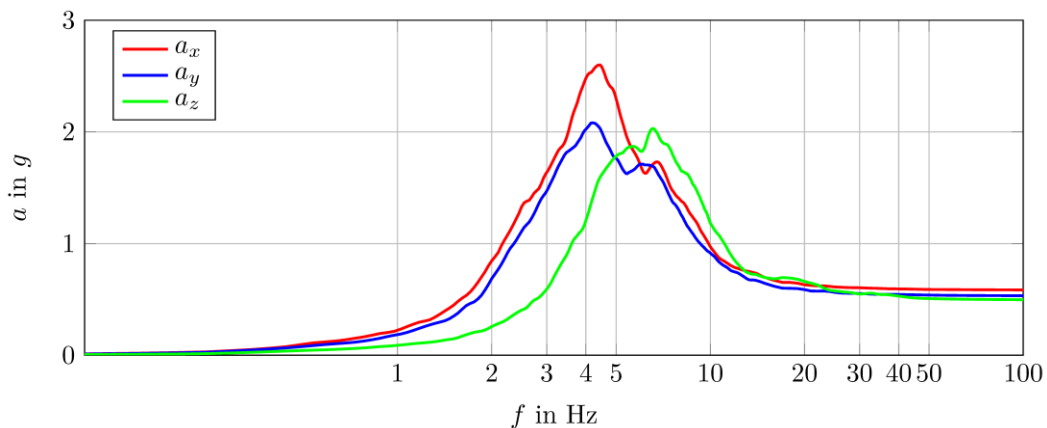


Figure 3: Floor response spectra on the pool ground for 5 % damping

MODEL

The simulations were performed with ANSYS Mechanical APDL, version 2019R3, on a Windows 10 platform. The model consists of the fuel storage rack, the water volume and the pool ground (Figure 4). The fuel storage rack stands on the rigid pool ground. The rack is surrounded by water. For the simulations,

the rack which is located closest to the pool wall is chosen, because this rack experiences the highest excitation by the dynamic fluid pressures and has the smallest distance to the pool wall. It has to be mentioned that the results of the simulations showed, that the accelerations of the fuel storage rack are small, which in turn means that the induced pressure waves have a small amplitude and the impact on the neighbouring racks is neglectable.

Fuel Pool

The fuel pool consists of fluid elements, which model linear acoustic waves. At the wetted surface between the water and the fuel storage rack, the structural elements and the fluid elements are coupled. The first sloshing frequencies are 0.32 Hz in x - and 0.35 Hz in y -direction. Considering Figure 3, the accelerations at these frequencies are very small. Consequently, the convective pressures are neglected. At the free water surface, a constant fluid pressure is defined. The remaining 5 outer surfaces of the pool are excited with the acceleration-time-histories.

Fuel Storage Rack

Solid shell and solid elements are used for the fuel storage rack - except for the pedestals and the fuel elements, which consist of beam and (ordinary) shell elements. The beam and (ordinary) shell elements are

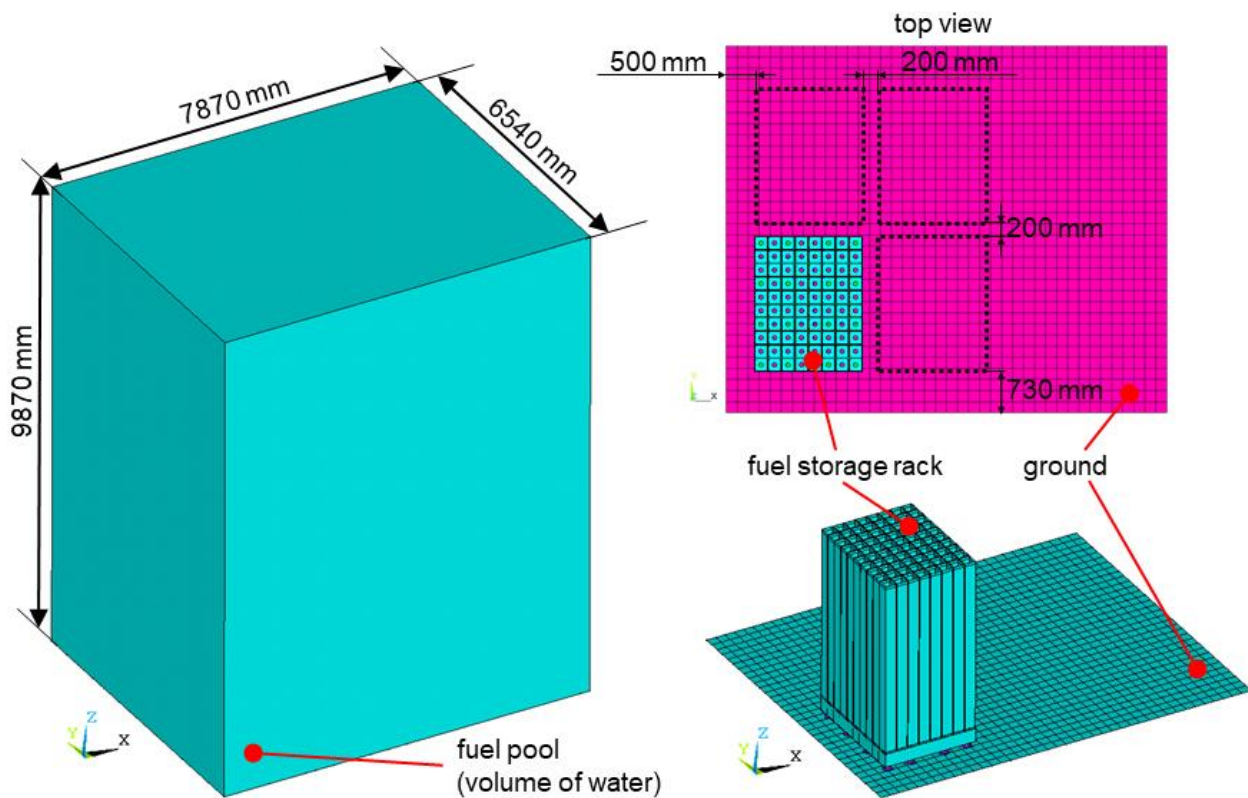


Figure 4: Model overview

not coupled with the fluid.

Considering the beams for the fuel elements, preliminary simulations with a detailed fuel element model were performed in order to obtain the stiffness characteristics. The results were used to define an equivalent cross section for the beam elements.

The fuel storage rack stands loosely on the pool ground (contact definition). The friction coefficient μ was varied between 0.2 and 0.8.

Between the beams of the fuel elements and the fuel element channels nonlinear springs are defined, where the distance between the head of the fuel element and the insert frame is 5 mm. Additionally, between the insert frames of the various fuel element channels also nonlinear springs are defined – here the distance between the insert frames is 1 mm. The stiffness of the springs is very small for tension and severely increases after the gap distance. Nevertheless, the spring stiffness for compression is not as high as the real contact stiffness, but this leads to higher displacements, which is conservative.

The total mass of the fully loaded fuel storage rack is ca. 54 tons (80 fuel elements 39 tons + rack 15 tons). The gravitational acceleration was adjusted to 8.66 m/s² in order to consider the effect of buoyancy. The rack is excited via the dynamic pressures and the accelerations of the pool ground.

Pool Ground

The pool ground consists of rigid shell elements, where, as already mentioned, contact is defined between the pool ground and the pedestals of the fuel storage rack. Every node of the pool ground is excited with the spectra-compatible acceleration-time-histories (x, y, z).

Material Properties

Nearly all components of the fuel storage rack are made of 1.4306. The maximum operating temperature of the fuel pool is 66 °C. Consequently, the material properties are:

- $R_{p0.2,66^\circ\text{C}} = 158.6 \text{ N/mm}^2$ (yield stress at 0.2 % plastic strain),
- $R_{p1.0,66^\circ\text{C}} = 187.2 \text{ N/mm}^2$ (yield stress at 1.0 % plastic strain),
- $R_{m,RT} = 450 \text{ N/mm}^2$ (tensile strength),
- $E_{66^\circ\text{C}} = 196720 \text{ N/mm}^2$ (modulus of elasticity),
- $\rho = 7900 \text{ kg/m}^3$ and
- $\nu = 0.3$ (Poisson ratio).

For the water of the fuel pool the following parameters were used:

- $\rho = 1000 \text{ kg/m}^3$ and
- $c = 1500 \text{ m/s}$.

The allowable stresses are calculated on the basis of ASME BPVC III Subsection NF (2017) and the application of ASME BPVC III Nonmandatory Appendix F (2017).

Linear Natural Frequencies and Damping

Linear natural frequency means, that for the modal analysis the nonlinear springs and contacts are not considered.

The natural frequencies are summarized in Table 1. It is obvious, that there is a high impact of FSI on the natural frequency of the fuel storage rack. By changing the fluid from air to water the frequency is shifted from 8.6 Hz to 3.4 Hz.

Simulations with the detailed model of a fuel element showed, that the effect of FSI on the natural frequency of the fuel element is neglectable. Consequently, it is reasonable to consider the fuel elements with beams, which are not coupled to the fluid.

Table 1: Linear natural frequencies of the fuel element and the fuel storage rack

	beam representing a fuel element	empty fuel storage rack (water)	empty fuel storage rack (air)
f_1 in Hz	2.2	3.4	8.6

The fuel storage rack mainly represents a welded construction. According to ASME BPVC III Nonmandatory Appendix N (2017) the damping ratio for this kind of construction for earthquake hazard is 4 %. The frequencies for the determination of the Rayleigh coefficients are 2 Hz and 100 Hz. The resulting coefficients are

- $\alpha = 0.986$ rad/s and
- $\beta = 1.248e-4$ s/rad.

The resulting damping curve is shown in Figure 5. The minimum damping ratio is 1.1 % for 14 Hz.

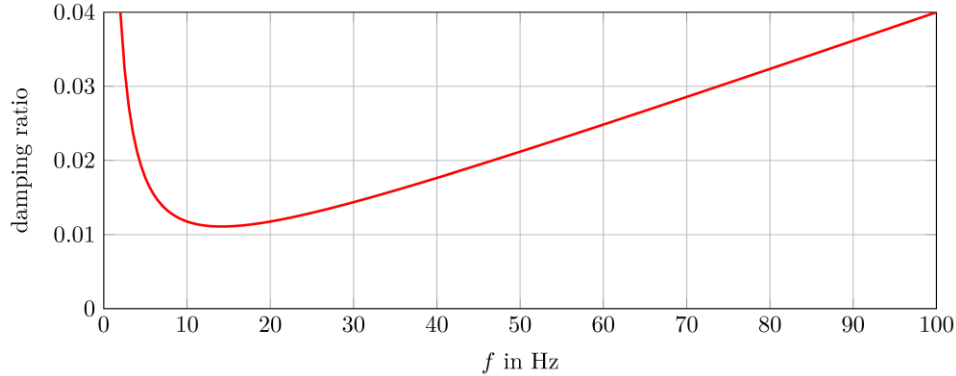


Figure 5: Damping ratio over frequency

Simulations

A summary of all performed simulations is given in Table 2. First of all, 7 simulations using the 7 spectra-compatible acceleration-time-histories (TH) are carried out (No. 1-7). For these calculations, a slightly higher time step of $\Delta t = 10$ ms was used in order to reduce the numerical effort. As a result of simulations 1-7, the TH with the highest relative displacement between the ground and the rack and the TH with the highest stresses are identified. Consequently, the TH with the highest stresses is recalculated using a smaller time step of $\Delta t = 2.5$ ms and additionally different friction coefficients (0.5 and 0.8).

Table 2: Simulation summary

No.	Δt in ms	μ	Comment
1-7	10	0.2	→ TH with highest displacements, TH with highest stresses
8	2.5	0.2	recalculation of TH with maximum stresses, $\Delta t = 2.5$ ms
9	2.5	0.5	recalculation of TH with maximum stresses, $\Delta t = 2.5$ ms, $\mu = 0.5$
10	2.5	0.8	recalculation of TH with maximum stresses, $\Delta t = 2.5$ ms, $\mu = 0.8$

RESULTS

As various simulations were carried out, the following section represents an extract of the most important results.

Relative Displacements (No. 1-7)

The maximum relative horizontal displacement is $u_{\max} = 51$ mm (Table 3, Figure 6). This value is much smaller than the minimum distance to the pool wall (500 mm) and the minimum distance between 2 neighbouring racks (200 mm). Consequently, collisions with other racks or the pool wall can be excluded. Figure 6 shows that the rack remains parallel to the pool walls. No rotation of the rack occurred. The

maximum vertical displacement is 6 mm – no severe tilting is observed. The relative standard deviation of the displacements is roughly 12 %.

Table 3: Maximum relative displacements including basic statistic values

u_{relative} in mm	u_{mean} in mm	u_{max} in mm	u_{min} in mm	standard deviation in mm	relative standard deviation in %
horizontal	42.4	51.1	36.9	5.4	12.9
vertical	5.2	6.0	4.2	0.6	11.6

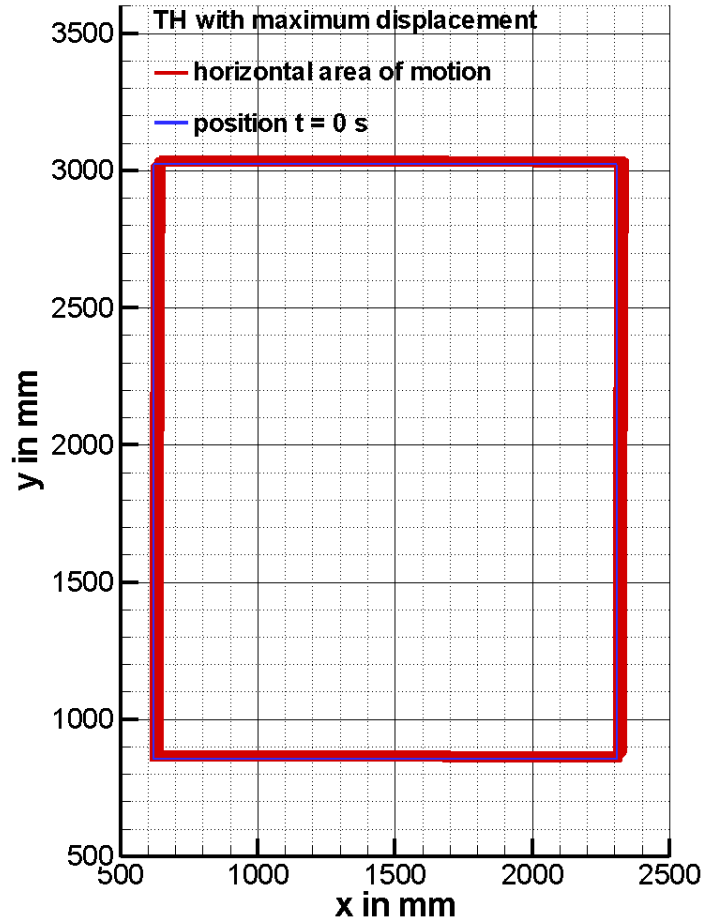


Figure 6: Horizontal area of motion for the simulation with the highest relative displacements (initial position is marked with a blue frame)

For higher friction coefficients, the amplitude of the relative displacements is smaller due to higher friction forces.

TH with the Highest Stresses (No. 8-10)

As a result of simulations No. 1-7 the acceleration-time-history, which causes the highest stresses, is identified. This setup is recalculated using a smaller time step of 2.5 ms and additional friction coefficients.

Figure 7 shows the distribution of the maximum stresses of the fuel storage rack for simulations No. 8-10. The stress distributions consider all nodes of the fuel element rack and all time steps. The increase

in stress from $\mu = 0.2$ to 0.5 is high ($98.8 \text{ N/mm}^2 \rightarrow 169.0 \text{ N/mm}^2$), in contrast to the increase of stress from $\mu = 0.5$ to 0.8 ($169.0 \text{ N/mm}^2 \rightarrow 177.9 \text{ N/mm}^2$), which is relatively small.

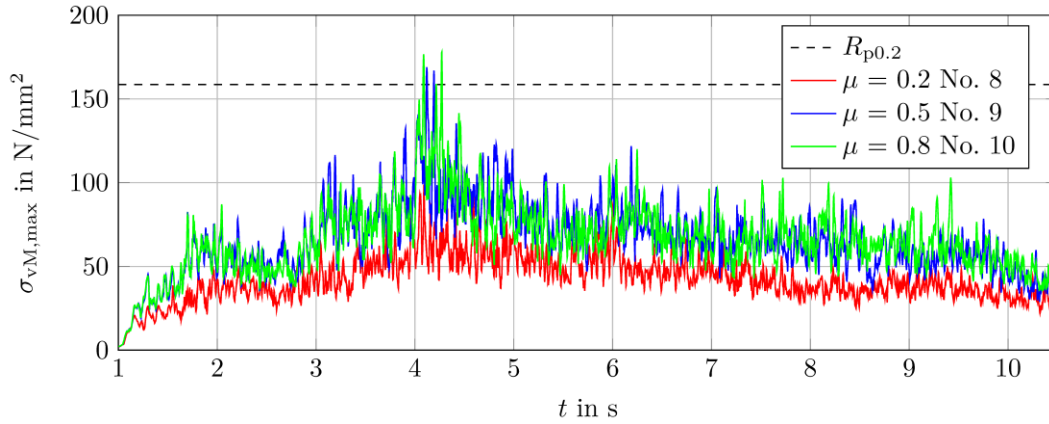


Figure 7: Maximum stress over time for simulations No. 8-10

For simulations No. 9 and 10, there are two short amplitudes which exceed the yield stress. Nevertheless, the occurring stresses are smaller than the allowable stresses. The maximum stresses are mainly caused by the bending of the fuel element channels.

Another effect of increasing the friction coefficient is an increase of the maximum vertical displacements (Table 4). The maximum vertical displacement of the fuel storage rack for a friction coefficient of 0.8 is 24.5 mm. As the base area of the rack is 2420 mm x 1930 mm, this maximum vertical displacement does not cause severe tilting.

Table 4: Maximum vertical and horizontal relative displacements for various friction coefficients

μ	u_{\max} in mm vertical	u_{\max} in mm horizontal
0.2	6.1	45.5
0.5	13.7	22.4
0.8	24.5	36.9

CONCLUSION

The seismic reevaluation of a fuel storage rack considering FSI and friction effects in consideration of a new earthquake hazard was positive. The new maximum accelerations are nearly 3 times higher than for the design of the fuel storage rack. The impact of FSI on the presented fuel storage rack is mainly a reduction of the natural frequency. Furthermore, when the rack oscillates pressure waves are generated (FSI) – this effect acts like additional damping for the fuel storage rack. For all performed simulations the maximum relative displacements are smaller than the minimum distance to the pool wall or neighbouring racks. Consequently, no collisions occurred. Additionally, no severe tilting is observed. For higher friction coefficients, the stress level increases, where the change in stress level from $\mu = 0.2$ to $\mu = 0.5$ is much higher than from $\mu = 0.5$ to $\mu = 0.8$. All in all, the occurring stresses are below the allowable stresses and the maximum fuel element accelerations are well below the allowable acceleration.

NOMENCLATURE

FSI	Fluid-Structure Interaction
TH	time-history
α	Rayleigh damping coefficient (mass proportional)
β	Rayleigh damping coefficient (stiffness proportional)
μ	friction coefficient
ρ	fluid density
ν	Poisson ratio
a	acceleration
c	speed of sound
f	frequency
g	gravitational acceleration
$p, \Delta p$	pressure, change in pressure
u	displacement
$v, \Delta v$	velocity, change in velocity
E	modulus of elasticity
H	pool height
L	half width of the fuel pool in direction of excitation
R_m	tensile strength
$R_{p0.2}$	yield stress at 0.2 % plastic strain
$R_{p1.0}$	yield stress at 1.0 % plastic strain

REFERENCES

- ASME BPVC III Nonmandatory Appendix N (2017). *Nonmandatory Appendix N – Article N-1000 Dynamic Analysis Methods*, ASME, New York, USA.
- ASME BPVC III Subsection NF (2017). *Division 1 – Subsection NF – Supports*, ASME, New York, USA.
- ASME BPVC III Nonmandatory Appendix F (2017). *Nonmandatory Appendix F – Article F-1000 – Rules for Evaluation of Service Loadings with Level D Service Limits*, ASME, New York, USA.
- Dehkharqani A. S., Aidanpää J.-O., Engström F. and Cervantes M. J. (2018). “A Review of Available Methods for the Assessment of Fluid Added Mass, Damping, and Stiffness With an Emphasis on Hydraulic Turbines”, *Applied Mechanics Reviews*, Volume 70, Issue 5, 20 pages.
- DIN EN 1998-4 (2007). *Eurocode 8: Design of structures for earthquake resistance – Part 4: Silos, tanks and pipelines*, CEN, Brussels, Belgium.
- IAEA (2015). *The Fukushima Daiichi Accident*, IAEA, Vienna, Austria.
- Joukowsky N. (1898). “Ueber den hydraulischen Stoss in Wasserleitungsröhren”, *Mémoires de l'Académie Impériale des Sciences de St.-Pétersbourg (1900)*, Series 8, 9:1-71, 1898. Complete paper presented to the Russian Technical Society, April 24, 1898.
- KTA 2201.1 (2011). *Auslegung von Kernkraftwerken gegen seismische Einwirkungen – Teil 1: Grundsätze*, Kerntechnischer Ausschuss, Salzgitter, Germany.